**International Journal of Power Electronics and Drive System (IJPEDS)**
Vol. 17, No. 2, June 2026, pp. 920~932
ISSN: 2088-8694, DOI: 10.11591/ijpeds.v17.i2.pp920-932 

# A neural learning algorithm for online rotor resistance estimation in sensorless induction motor drive systems

**Tuan V. Pham, Nguyen H. Thai**
Faculty of Electrical and Electronic Engineering, Vinh University of Technical Education, Vinh City, Viet Nam

**Article Info**

***Article history:***

Received Jul 25, 2025
Revised Mar 23, 2026
Accepted Apr 23, 2026

***Keywords:***

Artificial neural network
Fuzzy logic control
Model reference adaptive system
Rotor resistance estimation
Sensorless drives

**ABSTRACT**

This research proposes an advanced artificial neural network (ANN) framework optimized for the dynamic, real-time identification of rotor resistance (Rr) in sensorless induction motor (IM) drive systems. The proposed architecture introduces a self-tuning momentum factor within the neural learning update rule, which is adaptively modulated at each sampling interval. This modulation is governed by a Mamdani-based fuzzy inference system to ensure accelerated convergence and enhanced stability of the estimation process. Concurrently, the motor's angular velocity is estimated through a parallel ANN observer. Reliable identification of the time-varying rotor resistance is pivotal for compensating parametric sensitivity in flux observers, thereby optimizing the drive's control fidelity under varying thermal and load conditions. Comprehensive simulation and hardware-in-the-loop experimental results confirm that the proposed estimator tracks the actual Rr with high precision, maintaining steady-state errors within a 5% threshold.

*This is an open access article under the CC BY-SA license.*

***Corresponding Author:***

Nguyen H. Thai
Faculty of Electrical and Electronic Engineering, Vinh University of Technical Education
Vinh City, Viet Nam
Email: thainguyenktv@gmail.com

## 1. INTRODUCTION

In the contemporary landscape of industrial automation, high-performance sensorless control for three-phase induction machines has emerged as a critical research frontier [1]–[5]. For high-capacity industrial motors, the integration of mechanical speed transducers is often precluded by structural constraints or the susceptibility of encoders to electromagnetic interference and mechanical failures, particularly during low-speed, high-torque operations. The transition to sensorless topologies significantly mitigates system complexity and reduces the total cost of ownership while fortifying the drive against harsh operational environments, such as high thermal gradients and debris [6]–[9]. A fundamental challenge in sensorless field-oriented control (FOC) is the inherent sensitivity of the rotor flux observer to machine parameters, most notably the rotor resistance (Rr). This parameter is subject to significant drift up to 100% of its nominal value due to thermal-induced variations and changes in slip frequency [10]–[13]. Furthermore, the accuracy of the speed estimation process directly depends on the rotor flux value [14], [15]. Such parametric uncertainties lead to a mismatch between the controller's internal model and the physical plant, resulting in deteriorated torque dynamics and flux-weakening inaccuracies. Therefore, the implementation of a robust, online Rr estimation algorithm is essential for maintaining the asymptotic stability and dynamic performance of sensorless drives at low frequencies [10], [16]–[18].

The rotor resistance of an induction motor (IM) can vary by up to 100% due to the effects of temperature, rotor frequency, and the motor's operating conditions. This variation distorts the control model, adversely affecting torque and flux control capabilities, which in turn leads to reduced operational efficiency

and degraded dynamic response of the drive system. During the operation of the drive system, accurately determining the instantaneous value of rotor resistance using thermal models or temperature sensors poses a significant challenge. These methods require heavy computational resources, complex algorithm structures, and temperature sensors to be mounted directly at multiple points on the rotor, which is generally impractical in most industrial applications due to technical limitations and deployment costs [16], [19]–[23]. For these reasons, the research and development of online rotor resistance estimation algorithms for IM drive systems operating in the low-speed region are essential. It not only improves the control performance but also enhances the stability and reliability of the speed sensorless drive system in the low-speed region based on the field-oriented control method. Rotor resistance estimation algorithms have been extensively investigated in numerous published studies. Several methods proposed in the research are as follows: i) model reference adaptive system (MRAS) [17], [24]–[26], ii) extended Kalman filters (EKF) [8], [27]–[30], iii) sliding mode control (SMC) [10], [31], [32], and iv) fuzzy logic control (FLC) [33]–[35].

The proposed Rr estimator is integrated within an MRAS topology, where a voltage-based reference model and an ANN-based adaptive model operate in parallel. The ANN acts as a computational engine where its adjustable synaptic weights correspond directly to the motor's inverse rotor time constant [19], [36]. To mitigate the integration drift associated with back-EMF computation, a multi-stage cascaded low-pass filter (LPF) is employed in the reference flux observer, ensuring phase compensation and harmonic attenuation [37], [38].

This research proposes a sophisticated online identification scheme for induction motor rotor resistance, centered on a neural-network-based architecture. A pivotal innovation of the proposed estimator is the real-time modulation of the momentum factor, which is dynamically optimized at each sampling interval through a Mamdani-type fuzzy inference system (FIS). The manuscript is structured as follows: i) Section 1 provides a critical review of existing literature regarding rotor resistance tracking techniques; ii) Section 2 elucidates the design of the two-layer feedforward ANN and its fuzzy-logic-driven adaptation mechanism; and iii) Section 3 presents a rigorous performance evaluation utilizing both numerical simulations and experimental validation to verify the estimator's precision and stability.

## 2. ESTIMATION OF ROTOR RESISTANCE USING ANN

Rotor resistance estimation in an IM using an ANN is implemented within the MRAS framework, which includes two fundamental components: the voltage model (reference model) and the current model (adaptive model). In this approach, the ANN serves as the adaptive model. The neural network consists of both fixed and adjustable weights, where the adjustable weights are directly related to the rotor resistance value [19], [22], [36], [37], [39]. The block diagram of the rotor resistance estimator based on the MRAS configuration, employing an ANN trained with the backpropagation algorithm, is shown in Figure 1. In this structure, $R_{r\_es}$ denotes the estimated rotor resistance obtained from the neural network through the backpropagation learning process. The reference model, also known as the voltage model, provides the rotor leakage flux components in the stationary reference frame, as in (1).

$$\begin{cases} \psi_{r\alpha}^{v} = \frac{L_r}{L_m}[\int (V_{s\alpha} - R_s i_{s\alpha})dt - \sigma L_s i_{s\alpha}] \\ \psi_{r\beta}^{v} = \frac{L_r}{L_m}\left[\int \left(V_{s\beta} - R_s i_{s\beta}\right)dt - \sigma L_s i_{s\beta}\right] \end{cases} \quad (1)$$

$\sigma = (1 - L_m^2 / L_s L_r)$ - leakage coefficient. The (2) describes the stator leakage flux.

$$\begin{cases} \psi_{s\alpha} = \int (V_{s\alpha} - R_s i_{s\alpha})dt \\ \psi_{s\beta} = \int \left(V_{s\beta} - R_s i_{s\beta}\right)dt \end{cases} \quad (2)$$

Stator flux estimation accuracy is compromised by DC-link voltage pulsations, which introduce disturbances into the integrator defined in (2). As these errors accumulate over time, the reliability of the estimated flux components is significantly reduced. To mitigate this issue, a multi-stage low-pass filter (LPF) is employed, as suggested in [37], [38].

The transfer function of LPF, as in (3).

$$\frac{Y}{X} = \frac{1}{1 + j\tau\omega} \quad (3)$$

Where: $\zeta$ denotes the time constant, $\omega$ is the frequency of the input signal $X$; and $Y$ represents the output signal of the filter. From (2) and (3), and after several mathematical manipulations, the phase angle and magnitude of the transfer function are determined as (4) and (5) [37], [38].

$$\Phi = tan^{-1}(\zeta\omega) \tag{4}$$

$$K = \frac{1}{\sqrt{1+(\zeta\omega)^2}} \tag{5}$$

To estimate the stator flux, a series of three cascaded low-pass filters is utilized, as illustrated in Figure 2. The resultant phase displacement $\Phi_T$ and the total amplification factor $K_T$ of this filtering stage are calculated using (6) and (7).

$$\Phi_T = tan^{-1}(\zeta_1\omega) + tan^{-1}(\zeta_2\omega) + tan^{-1}(\zeta_3\omega) \tag{6}$$

$$K_T = K_1K_2K_3 \tag{7}$$

By assuming that the three filters are identical with a common time constant $\zeta_1 = \zeta_2 = \zeta_3 = \zeta$, the following relationships are derived as (8) and (9).

$$\Phi_T = 3\,tan^{-1}(\zeta\omega) \tag{8}$$

$$K_T = K^3 = \frac{1}{\left(\sqrt{1+(\zeta\omega)^2}\right)^3} \tag{9}$$

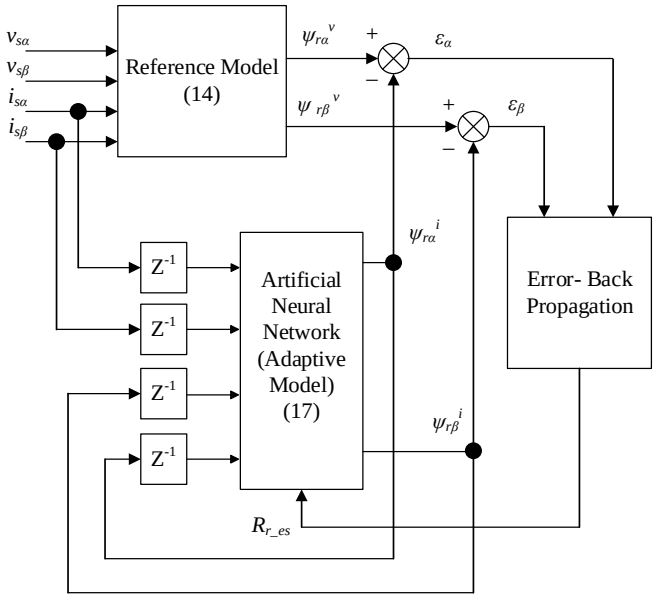


Figure 1. An ANN-based architecture for identifying rotor resistance parameters

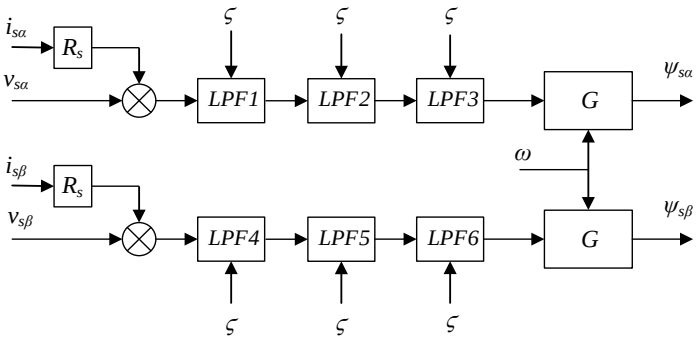


Figure 2. Architecture of the cascaded low-pass filter (LPF) used in stator flux identification [37], [38]

In order for the cascaded filter to function as an integrator, the following condition must be met:

$$\Phi_T = 90^0 \tag{10}$$

$$G.K_T = \frac{1}{\omega} \tag{11}$$

here, $G$ is the compensation gain.

$$\zeta = \frac{tan(90^0/3)}{\omega} \tag{12}$$

$$G = \frac{\left(\sqrt{[1+(\zeta\omega)^2]}\right)^3}{\omega} \tag{13}$$

Following the synthesis of (1) and (2), the resulting formulations for calculating the rotor flux within the reference model framework are established as (14).

$$\begin{cases} \psi_{r\alpha}^v(k) = \frac{L_r}{L_m}\psi_{s\alpha}(k-1) - \frac{L_sL_r-L_m^2}{L_m} i_{s\alpha}(k-1) \\ \psi_{r\beta}^v(k) = \frac{L_r}{L_m}\psi_{s\beta}(k-1) - \frac{L_sL_r-L_m^2}{L_m} i_{s\beta}(k-1) \end{cases} \tag{14}$$

In contrast, the adaptive model is mathematically represented by (15).

$$\begin{cases} \psi_{r\alpha}^i = \frac{1}{T_r}\int\left(L_m i_{s\alpha} - \psi_{r\alpha}^i - \omega_r T_r \psi_{r\beta}^i\right)dt \\ \psi_{r\beta}^i = \frac{1}{T_r}\int\left(L_m i_{s\beta} - \psi_{r\beta}^i + \omega_r T_r \psi_{r\alpha}^i\right)dt \end{cases} \tag{15}$$

By applying the discretization method to (16), we obtain:

$$\begin{cases} \frac{\psi_{r\alpha}^i(k)-\psi_{r\alpha}^i(k-1)}{T_s} = \frac{1}{T_r}\left(L_m i_{s\alpha}(k-1) - \psi_{r\alpha}^i(k-1) - \omega_r T_r \psi_{r\beta}^i(k-1)\right) \\ \frac{\psi_{r\beta}^i(k)-\psi_{r\beta}^i(k-1)}{T_s} = \frac{1}{T_r}\left(L_m i_{s\beta}(k-1) - \psi_{r\beta}^i(k-1) + \omega_r T_r \psi_{r\alpha}^i(k-1)\right) \end{cases} \tag{16}$$

Based on (16) and through a series of mathematical transformations, the following expression is derived:

$$\begin{cases} \psi_{r\alpha}^i(k) = W_1\psi_{r\alpha}^i(k-1) - W_2\psi_{r\beta}^i(k-1) + W_3 i_{s\alpha}(k-1) \\ \psi_{r\beta}^i(k) = W_1\psi_{r\beta}^i(k-1) + W_2\psi_{r\alpha}^i(k-1) + W_3 i_{s\beta}(k-1) \end{cases} \tag{17}$$

From the (17), an artificial neural network is constructed to estimate the rotor flux, as shown in Figure 3.

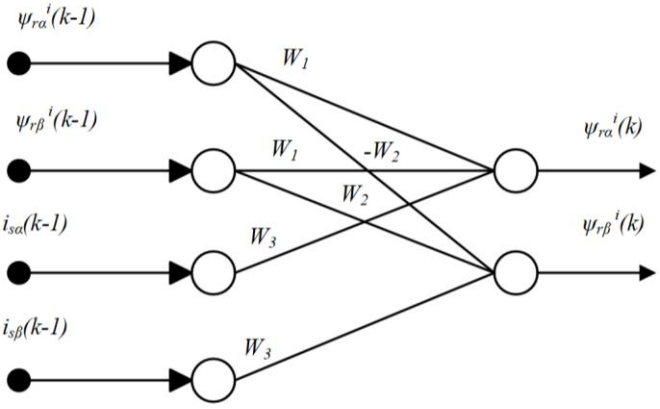


Figure 3. Two-layer artificial neural network used for rotor flux estimation

Where: $W_1 = 1 - \frac{T_S}{T_r}$, $W_2 = \omega_r T_s$ , $W_3 = \frac{T_S}{T_r} L_m$. Here, $T_s$ denotes the sampling period, and $T_r = \frac{L_r}{R_r}$. $W_1$ and $W_3$ are functions of the rotor time constant. $L_r$ remains unchanged. Therefore, the following relationship is obtained:

$$\begin{cases} W_1 = 1 - \frac{R_r T_S}{L_r} \\ W_3 = \frac{R_r T_S}{L_r} L_m \end{cases} \quad (18)$$

The training procedure aims to minimize the mean squared error (MSE) objective function E by tuning the weight matrices $W_1$ and $W_3$, following the approaches detailed in [36], [37]. The definition of the error $E$ is given by (19).

$$E = \frac{1}{2}\vec{e}^2(k) = \frac{1}{2}\left\{\overrightarrow{\psi_r^v}(k) - \overrightarrow{\psi_r^i}(k)\right\}^2 \quad (19)$$

$W_1, W_3$ are determined as (20) and (21).

$$W_1(k) = W_1(k-1) + \Delta W_1(k) + \alpha_1 \Delta W_1(k-1) \quad (20)$$

$$W_3(k) = W_3(k-1) + \Delta W_3(k) + \alpha_3 \Delta W_3(k-1) \quad (21)$$

With (22) and (23).

$$\Delta W_1(k) = -\frac{\partial E}{\partial W_1} = \left[\overrightarrow{\psi_r^v}(k) - \overrightarrow{\psi_r^i}(k)\right]\overrightarrow{\psi_r^i}(k-1) \quad (22)$$

$$\Delta W_3(k) = -\frac{\partial E}{\partial W_3} = \left[\overrightarrow{\psi_r^v}(k) - \overrightarrow{\psi_r^i}(k)\right]\overrightarrow{i_s}(k-1) \quad (23)$$

Where the momentum factor $\alpha_1$ and $\alpha_3$ are pre-selected constants. The problem addressed is to replace the constant momentum factor with a function such that, after each weight update, the error value $E$ is progressively reduced. Let $\varepsilon_i(k) = \Delta W_i(k)\,\Delta W_i(k-1)$, The function $\varepsilon_i(k)$ represents the product of the error and the weight i ($i$= 1 hoặc 3) at iterations k and (k−1). Based on the error product $\varepsilon_i(k)$, a momentum factor adaptation function is constructed such that the momentum factor is adjusted in a direction that reduces the network error $E$ (as defined in (18)):

– When $\varepsilon_i(k) > 0$, the neural network converges slowly, so the momentum factor should be increased.

– When $\varepsilon_i(k) < 0$, the neural network experiences overshooting, so the momentum factor should be decreased.

Figure 4 illustrates the block diagram using fuzzy logic to determine the momentum factor at the k-th sampling cycle. In this study, a fuzzy logic controller is proposed to determine the momentum factor of the neural network. The fuzzy logic system employs the Mamdani fuzzy inference model, which is chosen for its simplicity and ease of rule construction. The inputs to the fuzzy logic controller are the signals $\varepsilon_i(k)$ and $\Delta\varepsilon_i(k)$, as defined in Figures 5 and 6. The output is the adjustment value of the momentum factor, $\Delta\alpha_i(k)$, as shown in Figure 7. The fuzzy rules used in the controller are presented in Table 1.

The momentum factor value at the k-th sampling cycle is as (24).

$$\alpha_i(k) = \alpha_i(k-1) + \Delta\alpha_i(k) \quad (24)$$

The weights $W_1$ and $W_3$ are adjusted through training based on (19) and (20); with the momentum factor $\alpha_i(k)$ determined by (24). By transforming the system of (18), rotor resistance can be estimated using (25) or (26).

$$R_{r\_es} = \frac{L_r(1-W_1)}{T_s} \quad (25)$$

$$R_{r\_es} = \frac{L_r W_3}{L_m T_s} \quad (26)$$

The motor speed is estimated according to (27) [19].

$$\hat{\omega}(k) = \hat{\omega}(k-1) + \frac{\eta_w}{T_s}\left(\left[\psi_{r\beta}^v(k) - \psi_{r\beta}^i(k)\right]\psi_{r\alpha}^i(k-1) - \left[\psi_{r\alpha}^v(k) - \psi_{r\alpha}^i(k)\right]\psi_{r\beta}^i(k-1)\right) \quad (27)$$

Where $\eta_w$ is the learning rate. $\eta_w$ is usually chosen in the range (0 ÷ 1).

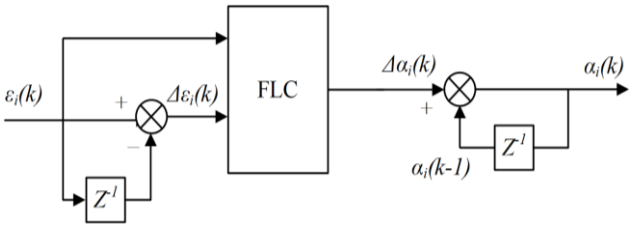


Figure 4. Block diagram using fuzzy logic to compute the momentum factor

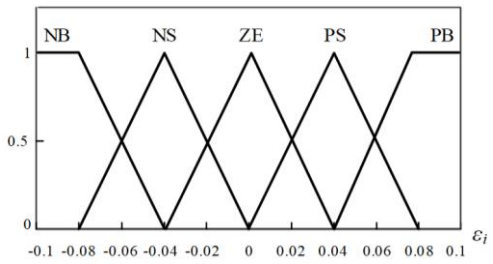


Figure 5. Graphical plots of the membership functions defining the fuzzy input $\varepsilon_i$

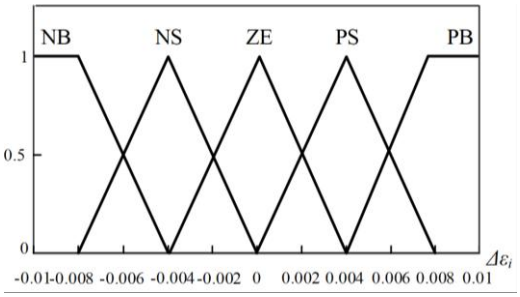


Figure 6. Graphical plots of the membership functions defining the fuzzy input $\Delta\varepsilon_i$

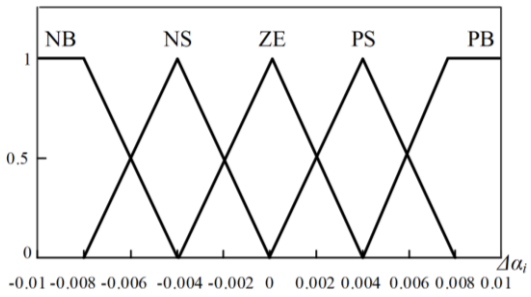


Figure 7. Graphical plots of the membership functions defining the fuzzy input $\Delta\alpha_i$

Table 1. Fuzzy logic rule

| Δε \ ε | NB | NS | ZE | PS | PB |
|---|---|---|---|---|---|
| NB | NB | NB | NS | ZE | PS |
| NS | NB | NS | ZE | PS | PS |
| ZE | NS | NS | ZE | ZE | PB |
| PS | NS | ZE | PS | PS | PB |
| PB | ZE | ZE | ZE | PB | PB |

## 3. RESULTS AND DISCUSSION

The rotor flux estimation based on (17) is highly sensitive to the rotor resistance [19]. Therefore, accurate rotor resistance estimation will enhance the performance of sensorless IM drives, particularly at low-speed operations. Figure 8 shows the sensorless IM drive using FOC controller with rotor resistance estimation. The momentum factor is determined using fuzzy logic controller (FLC). The motor parameters used in the simulation and experiments are presented in Table 2.

### 3.1. Result of the simulation

Table 2 summarizes the motor specifications utilized throughout the simulation studies. The proposed sensorless drive, incorporating a rotor resistance estimator, is developed and verified within the MATLAB/Simulink platform. To assess the estimator's robustness, the rotor resistance ($R_r$) is modeled with a 50% increase over its rated value, consistent with the scenarios in [16], [19]. Specifically, $R_r$ transitions from 1.84 Ω to 2.76 Ω during a 9-second interval. The system performance is evaluated under a constant speed command of 20 rad/s, with a step load torque of $T_L$ = 3.0 Nm introduced at t = 3.0 s.

#### 3.1.1. IM speed without rotor resistance estimation

The alignment between the estimated and reference speeds is presented in Figure 9(a). Despite a significant 50% deviation in rotor resistance from its initial value, Figure 9(b) confirms that the mean estimated speed remains constant at -20 rad/s. Furthermore, the speed ripple is kept within a minimal margin of nearly 0.6 rad/s, demonstrating the estimator's robustness against parameter variations. As illustrated in Figure 10, the proposed resistance observers in section 2 successfully converge to the actual rotor resistance with minimal error. This precise estimation directly contributes to the superior speed-tracking capabilities shown in Figure 11, where the measured speed aligns closely with the command value, validating the enhanced robustness of the drive system.

Table 2. IM parameters - siemens (1LA 7096-2AA60-Z)

| No | Parameters | Values | No | Parameters | Values |
|---|---|---|---|---|---|
| 1 | Reference power (Pn) | 2.2 kW | 5 | Magnetizing inductance (Lm) | 0.37 H |
| 2 | Reference voltage (Un) | 400 V | 6 | Poles (P) | 2 |
| 3 | Stator resistance (Rs) | 1.99 Ω | 7 | Reference speed (ωn) | 2880 Rpm |
| 4 | Rotor resistance (Rr) | 1.84 Ω | | | |

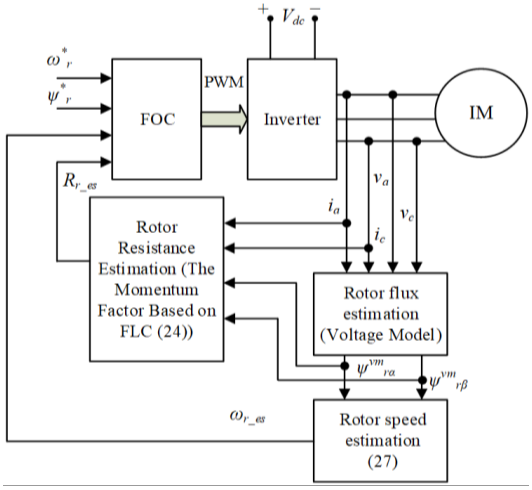


Figure 8. Proposed FOC-based sensorless drive topology with integrated ANN rotor resistance observer. The adaptation of the momentum factor is governed by a dedicated fuzzy logic supervisor

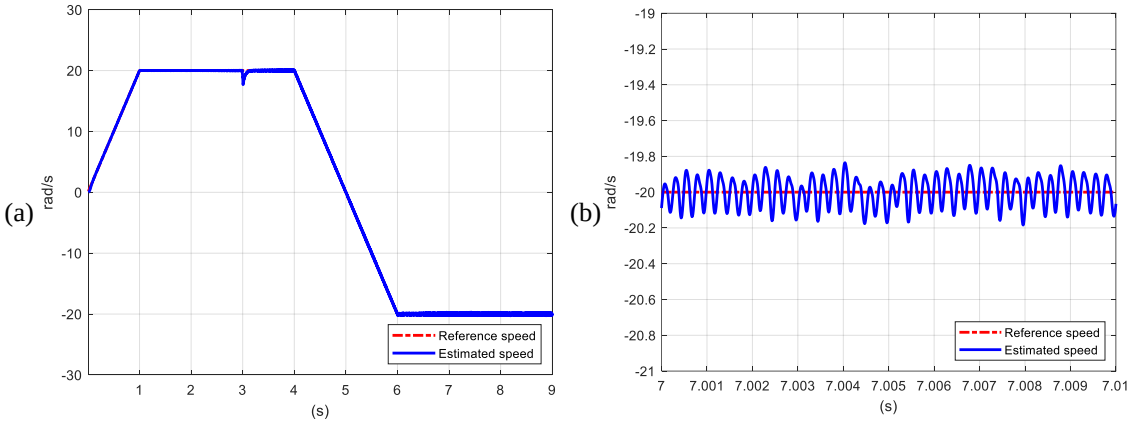


Figure 9. Motor speed consists of: reference speed and estimated speed of (a) throughout the entire simulation time and (b) during the simulation interval from 7.0 to 7.01 s

### 3.1.2. IM speed response under online rotor resistance adaptation

As illustrated in Figure 10, the proposed resistance observers in Section 2 successfully converge to the actual rotor resistance with minimal error. This precise estimation directly contributes to the superior speed-tracking capabilities shown in Figure 11, where the measured speed aligns closely with the command value, validating the enhanced robustness of the drive system.

### 3.2. Results of the experiment

The experimental verification is conducted on a dSPACE DS1104 platform (Figures 12 and 13). The system involves a three-phase IM (Table 2) coupled with a 1.5 kW DC motor. A Mentor II four-quadrant (4Q) rectifier operates the DC motor in torque control mode to apply the desired load to the IM.

A reference speed of 20 rad/s is utilized to evaluate the drive's low-speed performance [19]. In this setup, the momentum factor for the speed observer is set to $\eta_w = 0.1$. Based on preliminary experimental trials, the starting momentum factor for Rr estimation is chosen as $\alpha_r = 0.021$. Throughout the process, the machine operates against a load $T_L = 3.0$ Nm.

### 3.2.1. Estimated rotor resistance ($R_{r\_es}$)

As illustrated in Figure 14(a), the rotor resistance estimation (Rr_es) utilizing the momentum factor from (24) yields a mean value of approximately 2.07 Ω. Figure 14(b) shows that the estimator demonstrates high stability during operation. The observed fluctuations remain within 3% of the calculated average.

### 3.2.2. Drive system response without rotor resistance estimation

The reference speed is set at 20 rad/s. Figures 15(a) and 15(b) compare the reference speed with the measured speed, where the measured speed exhibits ripple relative to the reference value, with oscillations of approximately 6.5%. Figures 16(a) and 16(b) compare the reference speed with the estimated speed; the estimated speed fluctuates around the reference speed with an oscillation magnitude of approximately 9.6%. Figures 17 and 18 show that the αβ-axis flux estimated by the adaptive model has an amplitude approximately equal to that of the reference model flux, but exhibits a phase angle error.

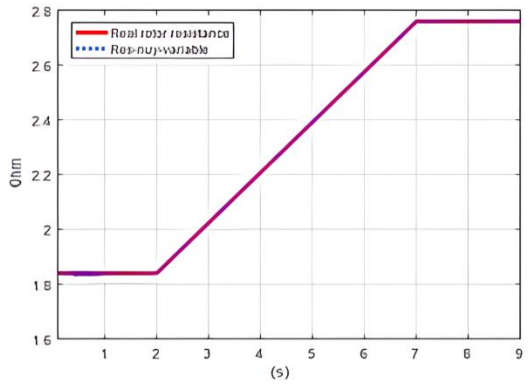


Figure 10. Comparison between the real rotor resistance and the estimated rotor resistance of the IM

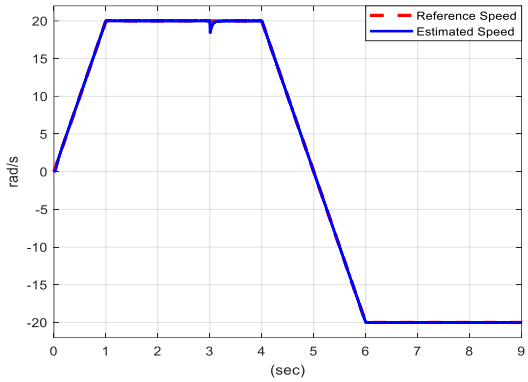


Figure 11. Speed response with online rotor resistance estimation, showing the reference speed and the estimated speed

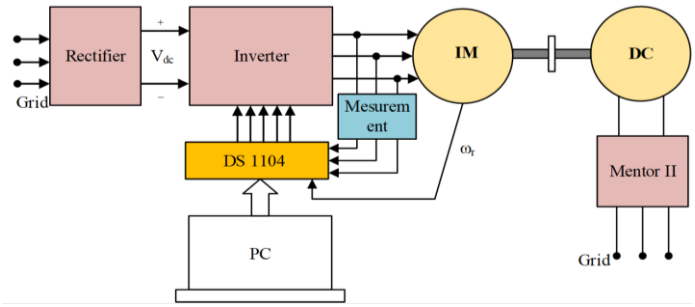


Figure 12. Schematic diagram of the experimental setup

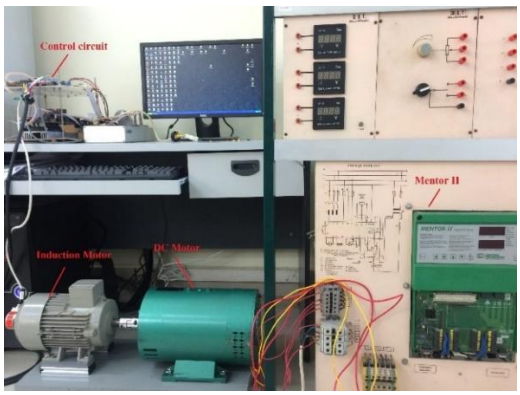


Figure 13. Photograph of the experimental setup

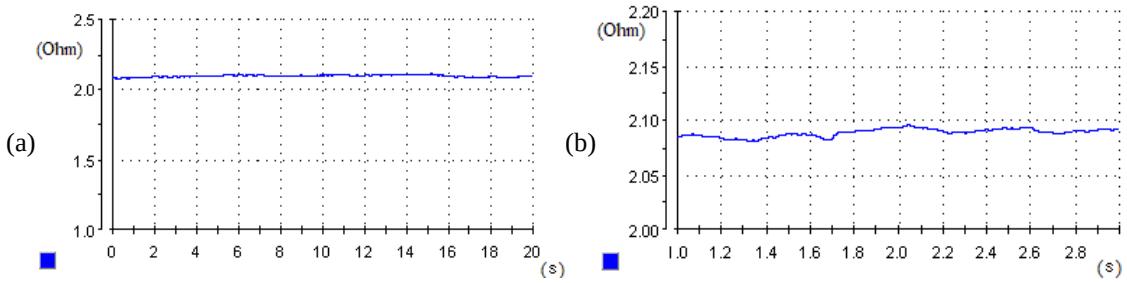


Figure 14. $R_{r\_es}$ with the momentum factor as a function (24): (a) over a 20-second measurement interval and (b) zoom of $R_{r\_es}$

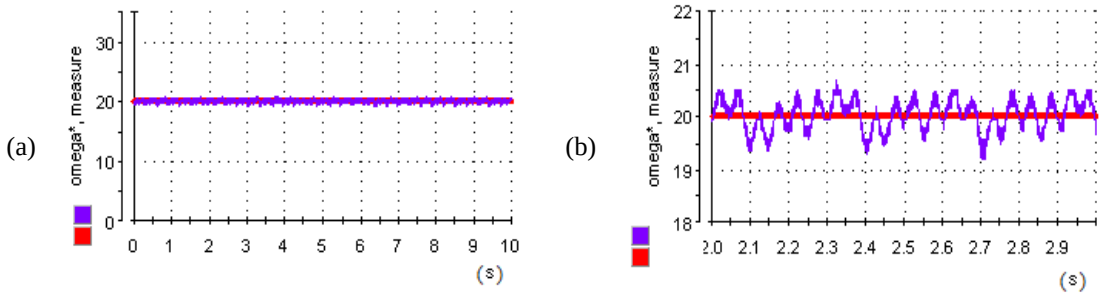


Figure 15. Motor speed, including reference speed and measured speed: (a) over a 10-second measurement interval and (b) over a 1-second measurement interval (from 2.0 to 3.0 s)

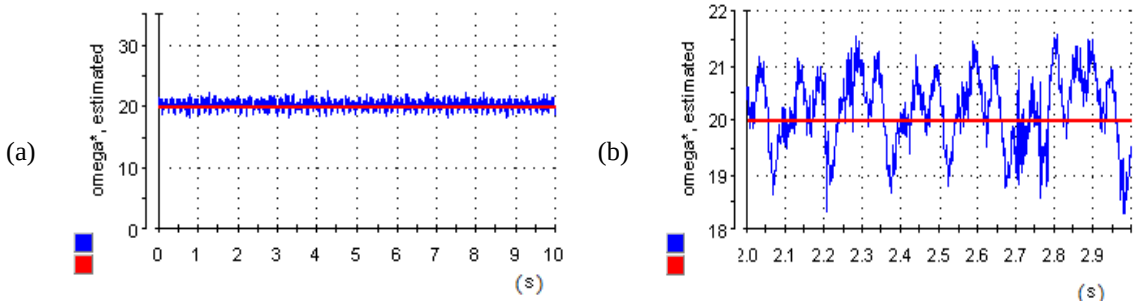


Figure 16. Motor speed, including reference speed and estimated speed: (a) over a 10-second measurement interval and (b) over a 1-second measurement interval (from 2.0 to 3.0 s)

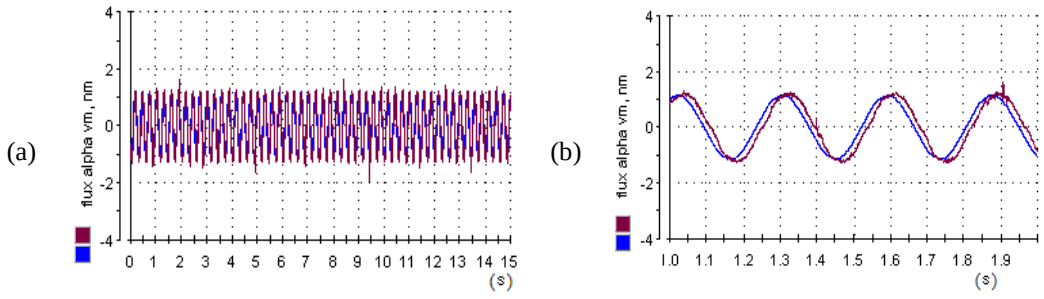


Figure 17. The rotor flux in the alpha axis includes: the model-based flux (in blue) and the adaptive neural-network-based flux (in purple): (a) over a 15-second measurement interval and (b) over a 1-second measurement interval (from 1.0 to 2.0 s)

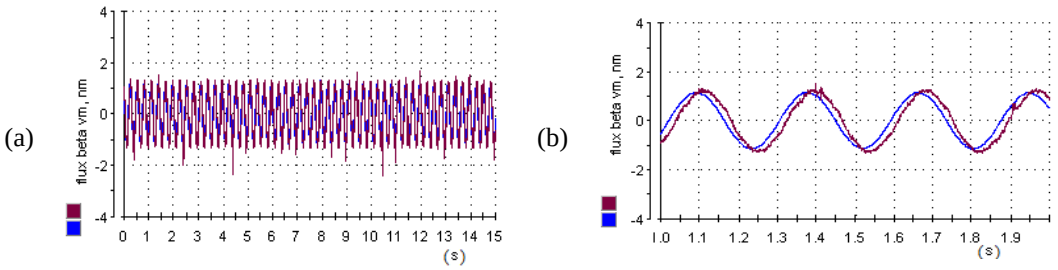


Figure 18. β-axis rotor flux components, showing the reference model flux (blue) and the adaptive neural network-estimated flux (purple): (a) over a 15-second measurement interval and (b) over a 1-second measurement interval (from 1.0 to 2.0 s)

### 3.2.3. Drive system response with online rotor resistance estimation

As illustrated in Figures 19(a) and 19(b), the actual speed exhibits high fidelity to the reference trajectory, with a ripple of approximately 2.0%. Figures 20(a) and 20(b) show that the estimated speed tracks the reference speed, with an error of approximately 5.0%. As illustrated in Figures 21 and 22, the estimated rotor flux components show excellent agreement with the reference model's values. This correlation proves that accurate Rr estimation leads to improved flux observer performance, providing empirical evidence for the theoretical insights discussed in section 2.

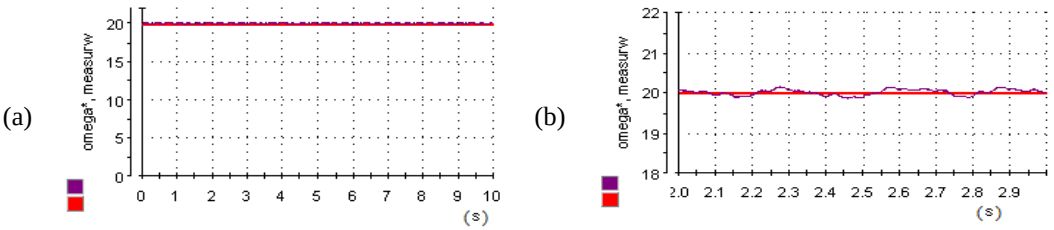


Figure 19. Motor speed, including reference speed and measured speed: (a) over a 10-second measurement interval and (b) over a 1-second measurement interval (from 2.0 to 3.0 s)

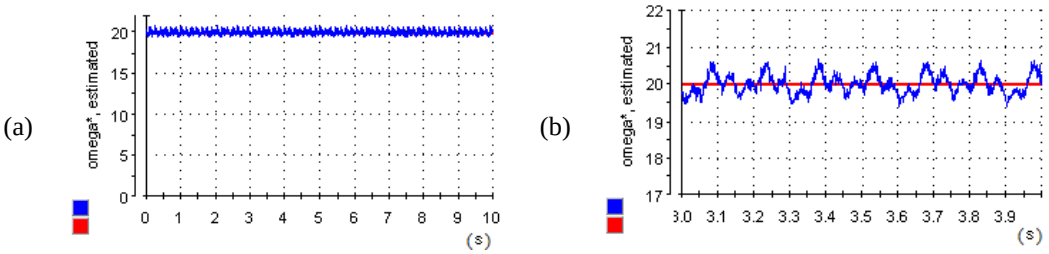


Figure 20. Motor speed, including reference speed and estimated speed: (a) over a 10-second measurement interval and (b) over a 1-second measurement interval (from 3.0 to 4.0 s)

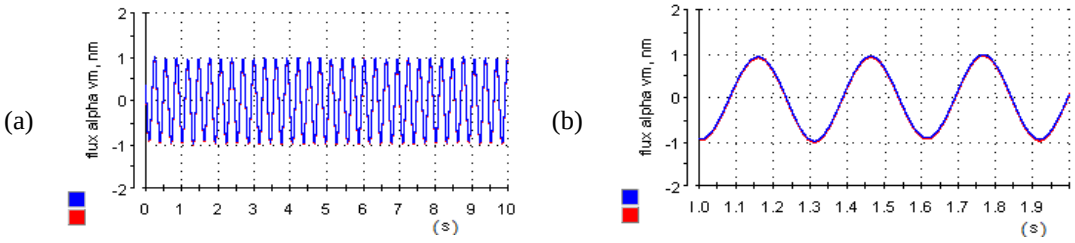


Figure 21. The rotor flux in the alpha axis includes: the model-based flux (in blue) and the adaptive neural-network-based flux (in purple): (a) over a 10-second measurement interval and (b) over a 1-second measurement interval (from 1.0 to 2.0 s)

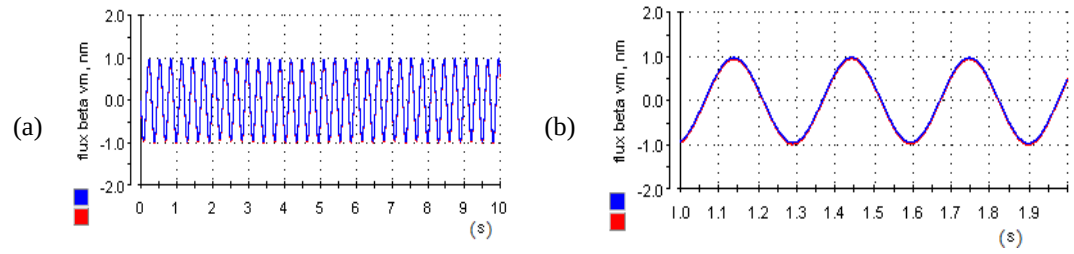


Figure 22. The rotor flux in the beta axis includes: the model-based flux (in blue) and the adaptive neural-network-based flux (in purple): (a) over a 10-second measurement interval and (b) over a 1-second measurement interval (from 1.0 to 2.0 s)

## 4. CONCLUSION

This paper successfully presents an advanced online rotor resistance identification strategy using an adaptive neural network integrated with a Mamdani-type fuzzy inference system for sensorless induction motor drives. Extensive simulation and experimental evaluations under severe parametric mismatch confirm that the proposed algorithm tracks time-varying resistance trajectories with high precision, maintaining steady-state estimation errors below 5,0%. By adaptively tuning the neural learning momentum, the proposed approach decouples the inherent trade-off between convergence speed and steady state ripple, reducing the actual speed regulation error to within 2,0% even under thermal drift and low-speed, heavily loaded disturbances. Consequently, robust flux observer decoupling and enhanced field-oriented control stability are achieved without requiring mechanical speed sensors.

Future research will address the limitation regarding the estimator's dependency on pre-identified machine parameters under deep magnetic saturation. Subsequent work will focus on developing a joint estimation framework that simultaneously tracks stator resistance, core losses, and rotor resistance to ensure comprehensive parametric robustness across the entire torque-speed operating envelope

## FUNDING INFORMATION

Authors state no funding involved.

## AUTHOR CONTRIBUTIONS STATEMENT

This journal uses the Contributor Roles Taxonomy (CRediT) to recognize individual author contributions, reduce authorship disputes, and facilitate collaboration.

| Name of Author | C | M | So | Va | Fo | I | R | D | O | E | Vi | Su | P | Fu |
|---|---|---|---|---|---|---|---|---|---|---|---|---|---|---|
| Tuan V. Pham | ✓ | ✓ | ✓ | ✓ | ✓ | ✓ | ✓ | ✓ | ✓ | ✓ | | | ✓ | |
| Nguyen H. Thai | | ✓ | | ✓ | | ✓ | ✓ | ✓ | ✓ | ✓ | ✓ | ✓ | | ✓ |

C : **C**onceptualization
M : **M**ethodology
So : **So**ftware
Va : **Va**lidation
Fo : **Fo**rmal analysis
I : **I**nvestigation
R : **R**esources
D : **D**ata Curation
O : Writing - **O**riginal Draft
E : Writing - Review & **E**diting
Vi : **Vi**sualization
Su : **Su**pervision
P : **P**roject administration
Fu : **Fu**nding acquisition

## CONFLICT OF INTEREST STATEMENT

Authors state no conflict of interest.

## DATA AVAILABILITY

The data that support the findings of this study are available from the corresponding author, [NHT], upon reasonable request.

## REFERENCES

[1] A. Dutt, A. Gauri, and V. B. R, "Sensorless direct torque control techniques for induction motor drives: a status review," in *2023 International Conference on Control, Communication and Computing (ICCC)*, IEEE, May 2023, pp. 1–6. doi: 10.1109/ICCC57789.2023.10165119.

[2] Q. Abdullah *et al.*, "Sensorless speed control of induction motor drives using reinforcement learning and self-tuning simplified fuzzy logic controller," *IEEE Access*, vol. 12, no. July, pp. 136485–136501, 2024, doi: 10.1109/ACCESS.2024.3435529.
[3] Y. Zhang, Z. Yin, W. Li, J. Liu, and Y. Zhang, "Adaptive sliding-mode-based speed control in finite control set model predictive torque control for induction motors," *IEEE Transactions on Power Electronics*, vol. 36, no. 7, pp. 8076–8087, 2021, doi: 10.1109/TPEL.2020.3042181.
[4] S. Krim, Y. Krim, and M. F. Mimouni, "Sensorless direct torque control based on nonlinear integral sliding mode controllers for an induction motor drive: Experimental verification," *Proceedings of the Institution of Mechanical Engineers. Part I: Journal of Systems and Control Engineering*, vol. 235, no. 2, pp. 249–268, 2021, doi: 10.1177/0959651820933733.
[5] H. Sharma, M. Saraswat, A. Yadav, J. H. Kim, and J. C. Bansal, Eds., *Congress on Intelligent Systems*, vol. 1334. in Advances in Intelligent Systems and Computing, vol. 1334. Singapore: Springer Singapore, 2021. doi: 10.1007/978-981-33-6981-8.
[6] R. Yildiz, M. Barut, and E. Zerdali, "A comprehensive comparison of extended and unscented Kalman filters for speed-sensorless control applications of induction motors," *IEEE Transactions on Industrial Informatics*, vol. 16, no. 10, pp. 6423–6432, 2020, doi: 10.1109/TII.2020.2964876.
[7] W. Xu, S. Qu, L. Zhao, and H. Zhang, "An improved adaptive sliding mode observer for middle- and high-speed rotor tracking," *IEEE Transactions on Power Electronics*, vol. 36, no. 1, pp. 1043–1053, 2021, doi: 10.1109/TPEL.2020.3000785.
[8] E. Zerdali, "A comparative study on adaptive EKF observers for state and parameter estimation of induction motor," *IEEE Transactions on Energy Conversion*, vol. 35, no. 3, pp. 1443–1452, 2020, doi: 10.1109/TEC.2020.2979850.
[9] J. Chen, Y. Fan, W. Wang, C. H. T. Lee, and Y. Wang, "Sensorless control for SynRM Drives using a pseudo-random high-frequency triangular-wave current signal injection scheme," *IEEE Transactions on Power Electronics*, vol. 37, no. 6, pp. 7122–7131, 2022, doi: 10.1109/TPEL.2022.3140829.
[10] A. Pyrkin, A. Bobtsov, A. Vedyakov, R. Ortega, A. Vediakova, and M. Sinetova, "A flux and speed observer for induction motors with unknown rotor resistance and load torque and no persistent excitation requirement," *International Journal of Adaptive Control and Signal Processing*, vol. 35, no. 8, pp. 1578–1593, 2021, doi: 10.1002/acs.3258.
[11] A. Balogun, A. Olajube, A. Awelewa, F. Okafor, T. Sanni, and I. Samuel, "A sensorless efficiency-optimizing vector control scheme for an induction motor drive," *Frontiers in Energy Research*, vol. 12, no. October, pp. 1–16, 2024, doi: 10.3389/fenrg.2024.1406565.
[12] W. T. Asfu, "Stator current-based model reference adaptive control for sensorless speed control of the induction motor," *Journal of Control Science and Engineering*, vol. 2020, 2020, doi: 10.1155/2020/8954704.
[13] I. Benlaloui, L. Chrifi-Alaoui, M. Ouriagli, A. Khemis, D. Khamari, and S. Drid, "Improvement of the induction motor sensorless control based on the type-2 fuzzy logic," *Electrical Engineering*, vol. 103, no. 3, pp. 1473–1482, 2021, doi: 10.1007/s00202-020-01178-1.
[14] A. Al-fahoum, "An applied approach for speed estimation of induction motors using sensorless flux observer system with sliding mode field oriented control," *International Journal of Electrical Engineering & Technology*, no. September, 2020, doi: 10.34218/IJEET.11.6.2020.011.
[15] M. S. Zaky and M. K. Metwaly, "Improved MRAS observer with rotor flux correction terms and FLC-based adaptive law for sensorless induction motor drives," *Scientific Reports*, vol. 15, no. 1, pp. 1–20, 2025, doi: 10.1038/s41598-025-98178-7.
[16] T. Pham Van, N. Thai Huu, H. Bui Thanh, and L. Nguyen Thanh, "Online rotor and stator resistance estimation using neural network for indirect vector controlled speed sensorless induction motor drive," *Proceedings of 2021 International Conference on System Science and Engineering, ICSSE 2021*, pp. 367–372, 2021, doi: 10.1109/ICSSE52999.2021.9538479.
[17] R. Kumar, V. P. Singh, and A. Mathur, *Intelligent algorithms for analysis and control of dynamical systems*. Springer Nature Singapore Pte Ltd, 2021. doi: doi.org/10.1007/978-981-15-8045-1.
[18] N. Patel, A. K. Bhoi, S. Padmanaban, and J. B. Holm-Nielsen, Eds., *Electric Vehicles*. in Green Energy and Technology. Singapore: Springer Singapore, 2021. doi: 10.1007/978-981-15-9251-5.
[19] T. P. Van, D. V. Tien, Z. Leonowicz, M. Jasinski, T. Sikorski, and P. Chakrabarti, "Online rotor and stator resistance estimation based on artificial neural network applied in sensorless induction motor drive," *Energies*, vol. 13, no. 18, 2020, doi: 10.3390/en13184946.
[20] S. Mao, H. Tao, and Z. Zheng, "Sensorless control of induction motors based on fractional-order linear super-twisting sliding mode observer with flux linkage compensation," *IEEE Access*, vol. 8, pp. 172308–172317, 2020, doi: 10.1109/ACCESS.2020.3024626.
[21] Y. P. Kuo and Y. C. Ji, "Sensorless adaptive rotor flux direct vector-controlled induction motor drive based on fuzzy logic control flux estimator," *Journal of Low Frequency Noise Vibration and Active Control*, vol. 40, no. 2, pp. 966–977, 2021, doi: 10.1177/1461348419842694.
[22] A. K. M. Kanakabettu, R. B. Irvathoor, S. Saralaya, S. B. Jodumutt, and A. B. Singh, "Novel advanced artificial neural network-based online stator and rotor resistance estimator for vector-controlled speed sensorless induction motor drives," *Energies*, vol. 17, no. 9, 2024, doi: 10.3390/en17092150.
[23] H. Che, B. Wu, J. Yang, and Y. Tian, "Speed sensorless sliding mode control of induction motor based on genetic algorithm optimization," *Measurement and Control (United Kingdom)*, vol. 53, no. 1–2, pp. 192–204, 2020, doi: 10.1177/0020294019881711.
[24] A. Diab, A. Abo El-Magd, and M. Abd El Sattar, "Design of a novel stator and rotor resistances estimator for sensorless induction motor drives," *Journal of Advanced Engineering Trends*, vol. 41, no. 2, pp. 284–293, 2021, doi: 10.21608/jaet.2021.210149.
[25] M. Adamczyk, "Rotor resistance estimator based on virtual current sensor algorithm for induction motor drives," *Power Electronics and Drives*, vol. 5, no. 1, pp. 143–156, 2020, doi: 10.2478/pead-2020-0008.
[26] M. S. Zaky and M. K. Metwaly, "Sensitivity analysis of a stator current-based MRAS estimator for sensorless induction motor drives," *Engineering, Technology and Applied Science Research*, vol. 14, no. 6, pp. 17584–17590, 2024, doi: 10.48084/etasr.8737.
[27] S. Udomsuk, K. Areerak, T. Areerak, and K. Areerak, "Online estimation of three-phase induction motor parameters using an extended Kalman filter for energy saving," *Energies*, vol. 17, no. 9, 2024, doi: 10.3390/en17092115.
[28] Q. Fu, L. Wang, Q. Xie, and Y. Zhou, "An improved adaptive iterative extended Kalman filter based on variational Bayesian," *Applied Sciences (Switzerland)*, vol. 14, no. 4, 2024, doi: 10.3390/app14041393.
[29] R. Inan and H. Bulent Ertan, "Rotor resistance estimation of induction motors with a novel innovation-based adaptive extended Kalman filter for self-tuning," *Proceedings of the International Conference on Optimisation of Electrical and Electronic Equipment, OPTIM*, 2023, doi: 10.1109/ACEMP-OPTIM57845.2023.10287080.
[30] B. Moaveni, Z. Masoumi, and P. Rahmani, "Introducing improved iterated extended Kalman filter (IIEKF) to estimate the rotor rotational speed, rotor and stator resistances of induction motors," *IEEE Access*, vol. 11, no. February, pp. 17584–17593, 2023, doi: 10.1109/ACCESS.2023.3244830.

[31] F. Stîngă, M. Marian, and D. Selișteanu, "Robust estimation-based control strategies for induction motors," *Complexity*, vol. 2020, 2020, doi: 10.1155/2020/9235701.
[32] S. A. Mansouri, A. Ahmarinejad, M. S. Javadi, R. Heidari, and J. P. S. Catalão, "Improved double-surface sliding mode observer for flux and speed estimation of induction motors," *IET Electric Power Applications*, vol. 14, no. 6, pp. 1002–1010, 2020, doi: 10.1049/iet-epa.2019.0826.
[33] R. Tidke and A. Chowdhury, "An experimental analysis of fuzzy logic-sliding mode based IFOC controlled induction motor drive," *AIMS Electronics and Electrical Engineering*, vol. 8, no. 3, pp. 340–359, 2024, doi: 10.3934/electreng.2024016.
[34] M. Zerikat, A. Mechernene, and S. Chekroun, "High-performance sensorless vector control of induction motor drives using artificial intelligent technique," in *2010 15th International Conference on Methods and Models in Automation and Robotics*, IEEE, Aug. 2010, pp. 67–75. doi: 10.1109/MMAR.2010.5587261.
[35] Y. Miloud and A. Draou, "Simulation analysis of a fuzzy logic based rotor resistance estimator of an indirect vector controlled induction motor drive," *Iranian Journal of Electrical and Computer Engineering*, vol. 4, no. 1, pp. 42–49, 2005.
[36] B. Karanayil, M. F. Rahman, and C. Grantham, "Online stator and rotor resistance estimation scheme using artificial neural networks for vector controlled speed sensorless induction motor drive," *IEEE Transactions on Industrial Electronics*, vol. 54, no. 1, pp. 167–176, 2007, doi: 10.1109/TIE.2006.888778.
[37] Baburaj Karanayil, *Parameter identification for vector controlled induction motor drives using artificial neural networks and fuzzy principles*. Theris submitted to The University of New South Wales for degree of Doctor of Philosophy, 2005.
[38] M. Koteich, "Flux estimation algorithms for electric drives: a comparative study," *2016 3rd International Conference on Renewable Energies for Developing Countries (REDEC)*, 2016, doi: 10.1109/REDEC.2016.7577558.
[39] D. Bielesz, M. Kubatko, Š. Kirschner, J. Milata, and V. Šotola, "Artificial neural network-based estimation for rotor-flux model reference adaptive system," *Transportation Research Procedia*, vol. 74, pp. 838–845, 2023, doi: 10.1016/j.trpro.2023.11.215.

## BIOGRAPHIES OF AUTHORS

**Tuan V. Pham** received the B.Eng., the M.S. degrees, and the Ph.D. degree in electrical engineering from Hanoi University of Science and Technology (HUST), Vietnam, in 2008, 2012, and 2020, respectively. He has worked as a lecturer in the Faculty of Electrical Engineering, Vinh University of Technology Education, Vinh, Vietnam. His research interests include electric machines and drives, power electronics, electrical motor parameter estimation, artificial intelligence, and machine learning. He can be contacted at email: tuanvp.bk@gmail.com.

**Nguyen H. Thai** received the B.Eng. degree in electrification and power supply and the M.Eng. degree in automation engineering from the Thai Nguyen University of Technology, Thai Nguyen, Vietnam, in 2001 and 2005, respectively, and the Ph.D. degree in control engineering and automation from the Hanoi University of Science and Technology, Hanoi, Vietnam, in 2015. Since 1996, he has been working at the Faculty of Electrical Engineering, Vinh University of Technology Education. His main research includes nonlinear adaptive control, fuzzy systems, neural networks, wireless sensor networks, mobile sensor networks, and robotics. He can be contacted at email: thainguyenktv@gmail.com.